AD-A128 040 OPTIMIZED COUPLERS BETWEEN JUNCTION LASERS AND SINGLE-MODE FIBERS(U) RCA LABS PRINCETON NJ J M HAMMER ET AL. MAR 83 RCA-PRRL-83-CR-4 1/1

UNCLASSIFIED SBI-AD-E001 425 N00014-81-C-2522 F/G 20/5 NL

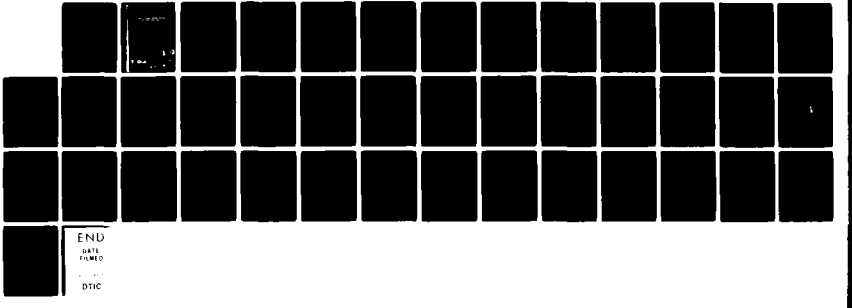

END

DATE FILMED

DTIC

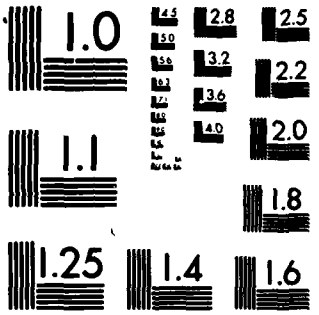

UNCLASSIFIED

SECURITY CLASSIFICATION OF THIS PAGE (When Data Entered)

REPORT DOCUMENTATION PAGE	READ INSTRUCTIONS BEFORE COMPLETING FORM
1. REPORT NUMBER	2. GOVT ACCESSION NO. AD-A128 040	3. RECIPIENT'S CATALOG NUMBER
4. TITLE (and Subtitle) OPTIMIZED COUPLERS BETWEEN JUNCTION LASERS AND SINGLE-MODE FIBERS	5. TYPE OF REPORT & PERIOD COVERED Final Report (8-31-81 to 1-31-83)
	6. PERFORMING ORG. REPORT NUMBER RCA-PRRL-83-CR-4
7. AUTHOR(s) J. M. Hammer and C. C. Neil	8. CONTRACT OR GRANT NUMBER(s) N00014-81-C-2522
9. PERFORMING ORGANIZATION NAME AND ADDRESS RCA Laboratories Princeton, New Jersey 08540	10. PROGRAM ELEMENT, PROJECT, TASK AREA & WORK UNIT NUMBERS
11. CONTROLLING OFFICE NAME AND ADDRESS Naval Research Laboratory Washington, DC 22217	12. REPORT DATE March 1983
	13. NUMBER OF PAGES 41
14. MONITORING AGENCY NAME & ADDRESS (If different from Controlling Office)	15. SECURITY CLASS. (of this report) Unclassified
	15a. DECLASSIFICATION/DOWNGRADING SCHEDULE N/A

16. DISTRIBUTION STATEMENT (of this Report)

This document has been approved for public release and sale; its distribution is unlimited.

17. DISTRIBUTION STATEMENT (of the abstract entered in Block 20, if different from Report)

18. SUPPLEMENTARY NOTES

19. KEY WORDS (Continue on reverse side if necessary and identify by block number)

Fibers	Single-mode fibers	Lightwave optics
Fiber coupling	Single-mode fiber coupling	
Diode lasers	Diode-laser coupling	
Laser coupling	Optical waveguide coupling	

20. ABSTRACT (Continue on reverse side if necessary and identify by block number) Single-mode fiber output power of over 7.5 mW cw has been obtained by the use of unique adjustable coupling modules that were developed for this program and that are being delivered to NRL. These are the highest powers ever reported coupled between diode lasers and single-mode fibers. Coupling efficiencies over 25% were obtained in simple butt-coupling by taking advantage of the large mode size available from RCA CDH-LOC lasers. We also observed peak fiber power of over 9 mW with 100-ns 50%-duty-cycle pulses.

DD FORM 1 JAN 73 1473

UNCLASSIFIED

SECURITY CLASSIFICATION OF THIS PAGE (When Data Entered)

20. The miniature modules provide relative transverse and lateral motion between fiber and laser with 2000-Å resolution, allowing fine tuning against long-term drifts. The coupling, while adjustable, is still stable against moderate acceleration of module and motion of fiber pigtail. The adjustments may be adapted to servo control. Still higher coupling efficiencies might be expected with cylinder lenses bonded to the fiber. Initial experiments indicated the need for further work to achieve accurate and stable attachment of lens to fiber.

PREFACE

This Final Report covers work performed at RCA Laboratories during the period 31 August 1981 to 31 January 1983 under Contract No. N00014-81-C-2522. This work was carried out in the Solid State Devices Laboratory, B. Hershenov, Director. The Group Head was M. Ettenberg, and the Project Scientist was J. M. Hammer.

The authors gratefully acknowledge the contributions made to this program by D. Botez and J. C. Connolly, who provided the CDH-LOC lasers used in the modules, and by M. G. Harvey and D. B. Gilbert, who helped select, mount, and characterize the lasers. They also wish to thank J. D. Morgan and the Staff of the RCA Model Shop for their careful fabrication of the mechanical components.

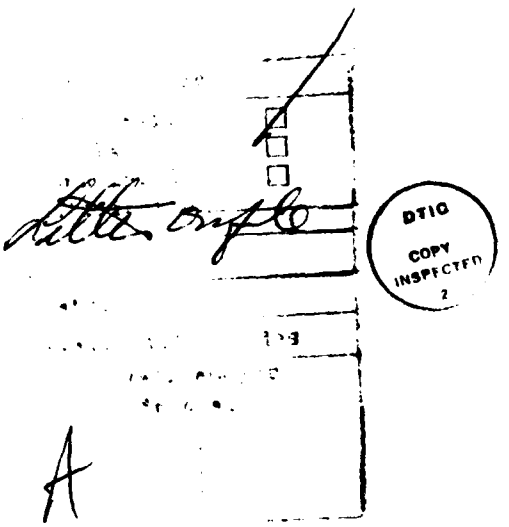

TABLE OF CONTENTS

Section		Page
I.	INTRODUCTION	1
II.	COUPLING THEORY	2
III.	DESIGN OF COUPLING MODULE	13
	A. Design Alternatives	13
	B. Calculation of Mechanical and Thermal Requirements	15
	C. Description of Complete Microcoupler Module	18
IV.	RESULTS AND DISCUSSION	21
	A. Module-Coupling Measurements	21
	B. Lens Coupling	29
V.	CONCLUSIONS	32
REFERENCES		33

LIST OF ILLUSTRATIONS

Figure		Page
1.	Schematic diagram for calculating coupling. A cross section in the x-z plane is shown. The laser junction lies in the y-z plane. The lens has a radius r_x and a refractive index n. The x offset is d_x, and the x tilt of the fiber axis is ϕ_x. The y-z plane may be represented by changing x subscripts to y subscripts. The fiber coordinate system is x_F,y_F (not shown), and z_F. z_F is in the x-z plane only when y tilt is zero	3
2.	Calculated coupling fraction K vs circular fiber beam waists ω_F for axial separations z = 0, 15, and 30 μm. Typical transverse laser beam waist ω_{Lx} = 0.65 μm, typical lateral laser beam waist ω_{Ly} = 2.40 μm, and typical wavelength λ = 0.84 μm	6
3.	Measured single-mode-fiber far-field tracing. The beam waists calculated from the far-field angles at P/2, P/e, and P/e^2 are 2.83, 2.85, and 2.83 μm, respectively. The average value 2.84 μm is used	7
4.	Calculated coupling fraction K vs offsets d_x and d_y for z = 0, 15, and 30 μm. The beam waists and wavelength of a typical CDH-LOC laser -- viz., ω_x = 0.65, ω_y = 2.40 μm, and λ = 0.84 μm -- are used. Measured fiber beam waist ω_F = 2.84 μm. These values are referred to as typical module values. $\phi_x = \phi_y = 0$	8
5.	Calculated coupling fraction K vs tilts ϕ_x and ϕ_y for z = 0, 15, and 30 μm for a typical module (see Fig. 4 caption) with $d_x = d_y = 0$	8
6.	Calculated coupling fraction K vs axial separation z for a typical module (see Fig. 4 caption). (a) d_x = 0, 1, and 2 μm; $d_y = \phi_x = \phi_y = 0$. (b) ϕ_y = 0, 2, and 4°; $d_x = d_y = \phi_x = 0$	9

LIST OF ILLUSTRATIONS (Continued)

Figure		Page
7.	Calculated coupling fraction K vs axial separation z for actual modules. d_x = 0, 1, and 2 μm; $d_y = \phi_x = \phi_y = 0$. ω_F = 2.84 μm. (a) Module MK2-0002: ω_{Lx} = 0.63, ω_{Ly} = 2.27, λ = 0.839 (μm); (b) Module MK2-0003: ω_{Lx} = 0.66, ω_{Ly} = 2.33, λ = 0.851 (μm); (c) Module MK2-0004: ω_{Lx} = 0.59, ω_{Ly} = 2.42, λ = 0.845 (μm); (d) Module MK2-0005: ω_{Lx} = 0.64, ω_{Ly} = 2.63, λ = 0.848 (μm)	10
8.	Calculated coupling vs z with lenses having a refractive index of n = 1.5. (a) Plano-convex spherical lens with lens radius values of 5, 10, 15, and 20 μm. (b) Plano-convex cylindrical lens with lens axis parallel to the lateral, y, direction. Lens radius values are r_x = 5, 10, 15, and 20 μm	11
9.	Schematic drawing of spring-loaded taper-screw microtranslator	15
10.	Calculated force required to deflect microtranslator of Fig. 9 vs deflection. Right-hand scale gives maximum stress. Upper scale gives number of turns of taper screw corresponding to deflection. The slope is 0.145 (kg-wt)/μm. The deflection plotted is at the laser-fiber holder position	17
11.	View of coupling module. A clamp and an electrical connection for the thermoelectric (TE) cooler are omitted for clarity	18
12.	CW fiber output vs laser current (solid line and left scale). Coupling fraction (round points and right scale). Coupling module MK2-0002	21
13.	CW fiber output vs laser current (solid line and left scale). Coupling fraction (round points and right scale). Coupling module MK2-0003	22

LIST OF ILLUSTRATIONS

Figure		Page
14.	CW fiber output vs laser current (solid line and left scale). Coupling fraction (round points and right scale). Module MK2-0004	23
15.	CW fiber output vs laser current (solid line and left scale). Coupling fraction (round points and right scale). Module MK2-0005	24
16.	Direct cw laser output vs current for the CDH-LOC laser used in Module MK2-0003. The soft "kink" in the 120- to 130-mA region is associated with the roll-off of coupling fraction in the modules	25
17.	Peak fiber output vs total laser current. The laser is operated with 80-mA, dc bias and 100-ns 50%-duty-cycle pulses. Module MK2-0004	26
18.	Far fields of the CDH-LOC laser used in Module MK2-0003. Note the difference in lateral far fields for I = 110 mA (10 mW) compared with I = 130 mA (20 mW)	28
19.	Calculated reflected power fraction vs axial separation z. A 4% Fresnel reflection from the fiber end facing the laser is assumed. The power fraction here is the fraction of the reflected light coupled into the laser mode for a typical CDH-LOC laser (see Fig. 4 caption)	29
20.	Spectrum of direct output from CDH-LOC laser used in Module MK2-0003. The current is 130 mA, dc. A single-wavelength mode remains over the range of currents studied	30
21.	Spectrum of fiber output at laser current of 110 mA, dc. Module MK2-0003. A single group of lines spaced at the laser-cavity/Fabry-Pérot separation is apparent	31
22.	Spectrum of fiber output at laser current of 130 mA, dc. Module MK2-0003. Compared with Fig. 21, a second group of lines appears	31

SECTION I

INTRODUCTION

In this report we describe the results of a program designed to produce modules in which high-power diode lasers are coupled to single-mode fibers. We have developed unique adjustable coupling modules in which more than 7.5 mW cw is available from the single-mode fiber pigtail. This is far higher than any result reported previously. The modules, while adjustable against long-term drifts in coupling, are stable so that normal handling presents no problem.

The results of a detailed application of the theory of coupling between Gaussian beams are given in Section II. These results have enabled us to define the parameters required for a stable coupling module. The design of a novel microtranslator capable of high-resolution adjustment within a module is presented in Section III. So is the method of using two of these microtranslators to construct the coupling module with both transverse and lateral adjustment capabilities. Our results and a discussion of these results are given in Section IV. Conclusions are presented in Section V.

SECTION II

COUPLING THEORY

This section contains a brief review of the theory of coupling between diode lasers and single-mode optical fibers and shows a detailed application of this theory to the needs of this program. We are using the well-known approach of considering the coupling between Gaussian beams [1]. As indicated below, the results of the theoretical calculation provide information necessary to choose the mechanical arrangement for positioning and holding the laser and the single-mode (SM) fiber.

There have been many theoretical treatments of the coupling between diode lasers and single-mode fibers [2-6]. We have chosen to follow the convenient and complete treatment published in 1980 by Sakai and Kimura [4]. Consider the arrangement shown in Fig. 1. The coordinates are shown in the x-z plane. An analogous figure could be used for the y-z plane. A lens of radius r_x is placed on the fiber end. The coupling fraction is found by calculating the overlap integral between the field of the laser at the end face of the fiber with the field that would exist in the fiber at its end face if it were guiding light. The calculation can include the effect of the lens placed at the fiber end face. Here, however, we first discuss the situation without a lens. We assign the coordinates x,z to the laser and the coordinates x_F,z_F to the fiber. These are shown in Fig. 1. The fiber coordinates may be tilted with respect to the laser coordinates by angles ϕ_x (ϕ_y) in the x-z (y-z) plane and displaced by distances d_x (d_y) in the x-z (y-z) plane. The displacement d_x is called x offset. The x direction is taken at right angles; the y direction, parallel to the laser junction plane. The x direction here is thus what is commonly referred to as the transverse direction, and the y direction coincides with what is commonly referred to as the lateral direction.

In these coordinates the x component of the field of the laser beam in the plane of the fiber end face may be represented as

$$E_L^{(x)}(x,z) = \frac{\omega_{Lx}}{\omega_x} E_{L0} \exp\left[- \frac{x^2}{\omega_x^2} + j\, \Omega^x(x,z) \right]$$

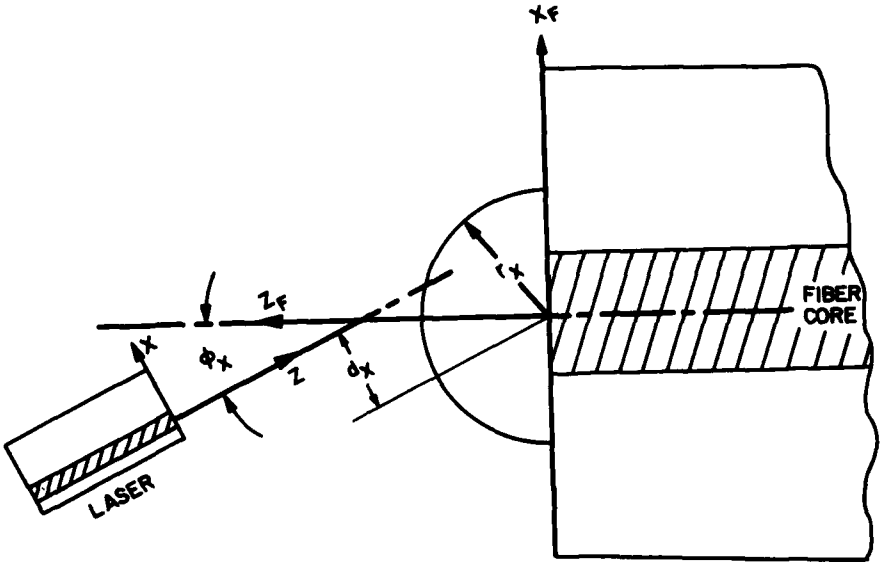

Figure 1. Schematic diagram for calculating coupling. A cross section in the x-z plane is shown. The laser junction lies in the y-z plane. The lens has a radius r_x and a refractive index n. The x offset is d_x, and the x tilt of the fiber axis is ϕ_x. The y-z plane may be represented by changing x subscripts to y subscripts. The fiber coordinate system is x_F, y_F (not shown), and z_F. z_F is in the x-z plane only when y tilt is zero.

Similarly, in the y-z plane,

$$E_L^{(y)}(y,z) = \frac{\omega_{Ly}}{\omega_y} E_{L0} \exp\left[- \frac{x^2}{\omega_y^2} + j\, \Omega^x(y,z) \right]$$

where

$$\omega_x = \omega_{Lx} \sqrt{1 + \left(\frac{2z}{k\omega_{Lx}^2} \right)^2}$$

$$\omega_y = \omega_{Ly} \sqrt{1 + \left(\frac{2z}{k\omega_{Ly}^2} \right)^2}$$

$k = 2\pi/\lambda$, and

$j = \sqrt{-1}$

$2\omega_{Lx}$ and $2\omega_{Ly}$ are the dimensions of the laser beam at the beam waist measured to the $1/e^2$ power points. We assume that the beam waists are located at the laser facet. In terms of the asymptotic far-field angles of a Gaussian beam, ω_{Lx} and ω_{Ly} may be found from

$$\omega_{Lx} = \frac{1}{2k \tan (\theta_x/2)}$$

$$\omega_{Ly} = \frac{1}{2k \tan (\theta_y/2)}$$

The complete representation of the field including the phase factors $\Omega^x(x,z)$ and $\Omega^y(y,z)$ is given by Sakai and Kimura [4] and is not repeated here. The tilt angles and the offsets are, however, included in Ω^x and Ω^y. The field of the fiber at the fiber end is given in terms of the laser coordinates by

$$E_F^{(x)}\ (x, z_F = 0) = E_{F0} \exp\left[-(d_x + x)^2/\omega_{Fx}^2\right] \text{ and}$$
$$E_F^{(y)}\ (y, z_F = 0) = E_{F0} \exp\left[-(d_y + y)^2/\omega_{Fy}^2\right]$$

$2\ \omega_{Fx}$ and $2\ \omega_{Fy}$ are the beam waists of the single fiber mode that we assume to be located at the fiber end face. Thus, the theory can encompass noncircular fibers.

The transverse (x direction) coupling fraction $K^{(x)}$ is given by

$$K^{(x)} = \frac{\left| \int_{S_F} E_L^{(x)}(x,z) \cdot \left[E_F^{(x)}(y, z_F = 0) \right]^* dS_F \right|^2}{\int_S \left| E_L^{(x)}(x,0) \right|^2 dS_L \int_{S_F} \left| E_F^{(x)}(y, z_F = 0) \right|^2 dS_F}$$

The integration of the overlap integral (the numerator) is taken over the fiber end face as indicated by S_F. The denominator normalizes the power. Here the laser field is integrated over the laser facet indicated by S_L, and the fiber

field over the fiber end face. An analogous expression is used for the lateral (y direction) coupling $K^{(y)}$. The total coupling fraction is given by

$$K = K^{(x)}\ K^{(y)}$$

The integration is performed and the result given in closed form in Ref. 4. It is convenient for computation to write the solution given there as follows:

Define $W_1 = \omega_{Lx}$; $U = \omega_{Fx}$

$$W = \left(\sqrt{4z^2 + kW_1^2}\right)/kW_1$$

$$R = (4z^2 + kW_1^2)^2/4z$$

$$A = 1/W^2 + 1/U^2$$

$$B = k/2R$$

$$C = A^2 + B^2$$

$$N_1 = 2/(WU\sqrt{C})$$

$$N_2 = \exp\{-2d^2/(U^2)[1 - A/(U^2C)]\}$$

$$N_3 = \exp\{-(\phi_x n_0 k)^2\ A/(2C)\}$$

$$N_4 = \exp\{2d\phi_x n_0\ kB/(U^2C)\}$$

$$K^{(x)} = N_1N_2N_3N_4$$

Analogous expressions are used for $K^{(y)}$.

If a plano-convex lens with refractive index n and radius r_x in the x-z (r_y in the y-z) plane is placed on the fiber end, the coupling efficiency, for the case of zero tilt and offset, is

$$K^{(x)} = 2/\ WU\left\{\sqrt{A^2 + [B - (n - 1)k/(2r_x)]^2}\right\}$$

The analogous expression may be used for $K^{(y)}$. This is the same as the expression used by Ladany et al. [3]. The complete expression including tilt and offset when a lens is used is given by Sakai and Kimura [4].

We have used these expressions to plot coupling fraction as a function of various parameters of interest in designing our coupling module. For all of these plots we have assumed a circular fiber so that $\omega_{Fx} = \omega_{Fy} = \omega_F$.

Typical CDH-LOC lasers [7,8] employed in our program have w_{Lx} = 0.65 μm, w_{Ly} = 2.4 μm, and λ = 0.84 μm. Figure 2 is a plot of total coupling fraction K against the fiber beam waist w_F. The axial separation distance z is the parameter. Curves for z = 0, 15, and 30 μm are given. At z = 0, a maximum fractional coupling of 0.7 would be obtained for a fiber with $w_F \sim 1.0$ μm. At z = 15 μm, the coupling fraction varies slowly around a peak of 0.4 for fibers with w_F in the range of 2-3 μm. Single-mode fibers in this range are commercially available. In addition, an axial spacing of 10-20 μm is readily achieved and maintained. Closer spacings pose laser-mounting and mechanical-stability problems. We thus chose as our principal fiber a single-mode fiber manufactured by Corning Glass Works (43650-V01), whose beam waist we determined from the far-field measurements [9] shown in Fig. 3 to be w_F = 2.84 μm. The fiber with the smallest mode size available to us was an ITT fiber, T1605, with a calculated beam waist at 0.84 μm of 2.3 μm. It is, however, a polarization-conserving fiber and proved difficult to handle. Besides, it offered us only a marginal potential improvement in coupling.

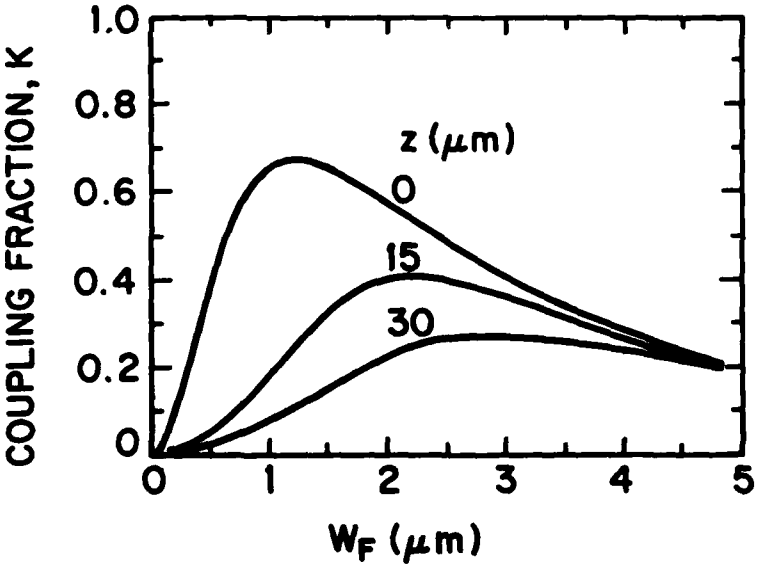

Figure 2. Calculated coupling fraction K vs circular fiber beam waists w_F for axial separations z = 0, 15, and 30 μm. Typical transverse laser beam waist w_{Lx} = 0.65 μm, typical lateral laser beam waist w_{Ly} = 2.40 μm, and typical wavelength λ = 0.84 μm.

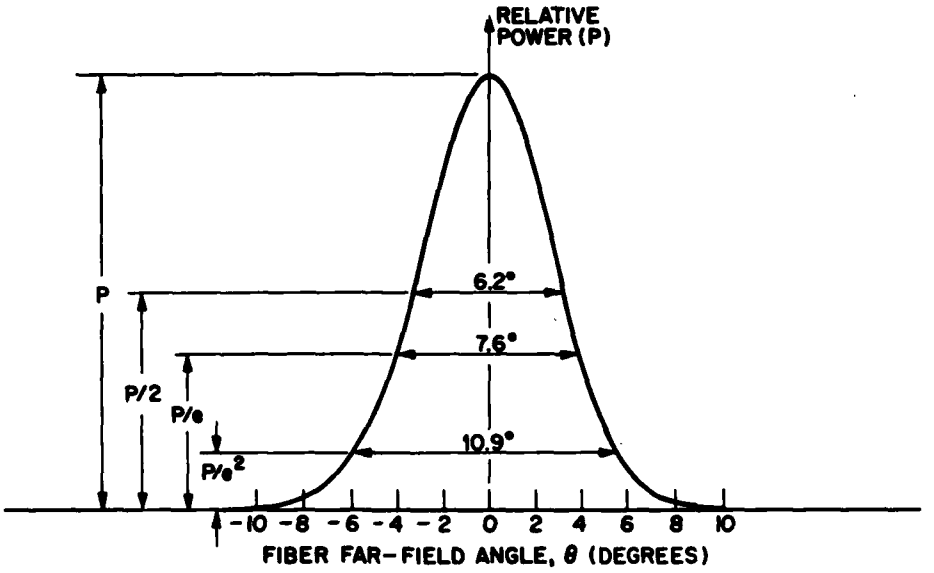

Figure 3. Measured single-mode-fiber far-field tracing. The beam waists calculated from the far-field angles at P/2, P/e, and P/e^2 are 2.83, 2.85, and 2.83 μm, respectively. The average value 2.84 μm is used.

Figures 4(a) and 4(b) give total coupling fraction K as a function of x-offset d_x and y-offset d_y, respectively, for a typical laser coupled to the Corning 43650-V01 fiber (ω_F = 2.84 μm). Curves for z = 0, 15, and 30 μm are given. The tilt angles are zero. At z = 15 μm, offsets in the transverse direction, d_x, are more damaging than offsets in the lateral direction, d_y. This might be expected from a laser beam waist size that is narrower in the transverse than in the lateral direction. K falls from 0.37 at d_x = 0 to 0.3 at d_x = 1 μm. K drops by 50% at d_x = 2 μm and vanishes at approximately d_x = 5 μm. Thus, it is clear that the transverse position must be controlled to fractions of a micrometer to achieve stable coupling. Figure 5(a) plots K against transverse-tilt angle ϕ_x, and Fig. 5(b) plots K vs lateral-tilt angle ϕ_y. Axial distance z is again the parameter. Curves for z = 0, 15, and 30 μm are shown. Here, too, beam waists for a typical laser and the 43650-V01 fiber are used; the offset is zero.

It is interesting that lateral tilt ϕ_y is more damaging than transverse tilt ϕ_x. This is in contrast to offset and is readily understood since the lateral laser far-field angle is much smaller than the transverse angle. At

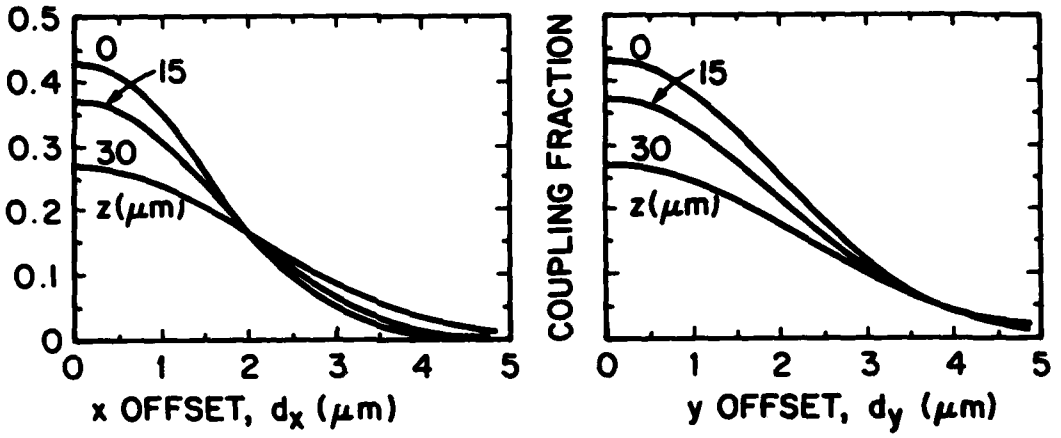

Figure 4. Calculated coupling fraction K vs offsets d_x and d_y for $z = 0$, 15, and 30 μm. The beam waists and wavelength of a typical CDH-LOC laser -- viz., $\omega_x = 0.65$, $\omega_y = 2.40$ μm, and $\lambda = 0.84$ μm -- are used. Measured fiber beam waist $\omega_F = 2.84$ μm. These values are referred to as typical module values. $\phi_x = \phi_y = 0$.

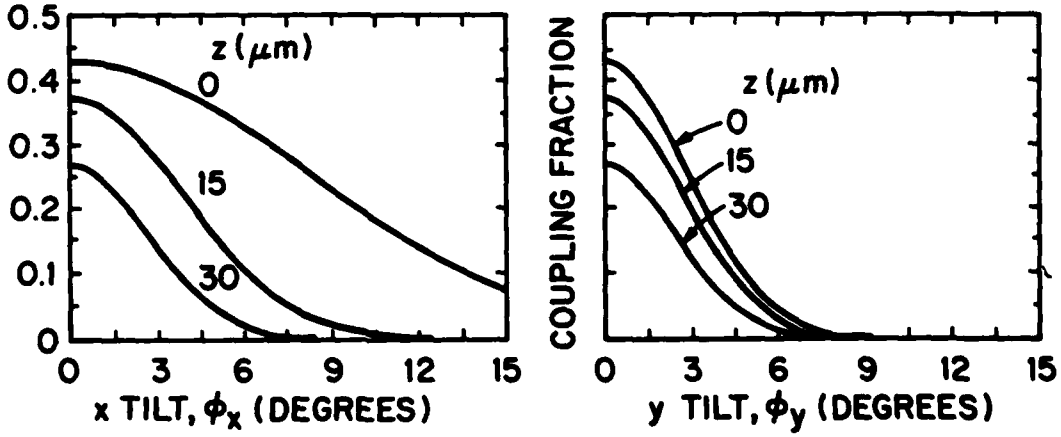

Figure 5. Calculated coupling fraction K vs tilts ϕ_x and ϕ_y for $z = 0$, 15, and 30 μm for a typical module (see Fig. 4 caption) with $d_x = d_y = 0$.

$z = 15$ μm, a tilt of 1.5° reduces the coupling from 0.37 to about 0.3. Three degrees of lateral tilt halve the coupling; at $\phi_y = 8°$, the coupling substan-

tially vanishes. We might say that 1.5° of lateral tilt is as bad as 1 μm of transverse offset and vice versa.

In Fig. 6(a) the coupling fraction for a typical laser is plotted vs axial separation z for transverse offsets d_x = 0, 1, and 2 μm; $\phi_{x,y}$ = 0. Figure 6(b) shows K vs z for ϕ_y = 0, 2, and 4°, with d_x and d_y equal to zero. The change in coupling with z is relatively small in all cases. K drops from its maximum value of approximately 0.43 at z = 0 with zero offset and tilt to 0.37 at z = 15 μm. The average distance chosen in constructing the modules is z = 10 μm. It is interesting to note that the coupling increases slightly from z = 0 to z = 20 μm for large offsets, as shown by the curve for d_x = 2 μm.

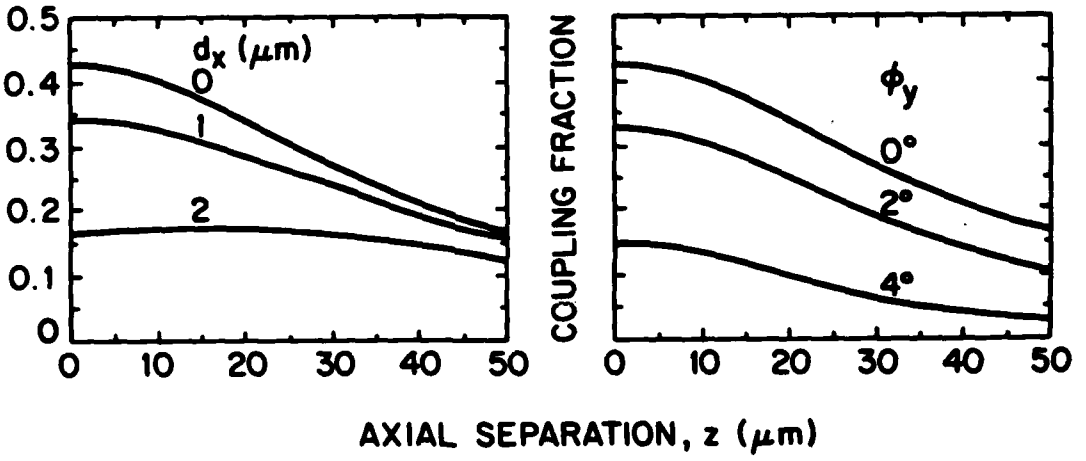

Figure 6. Calculated coupling fraction K vs axial separation z for a typical module (see Fig. 4 caption). (a) d_x = 0, 1, and 2 μm; $d_y = \phi_x = \phi_y = 0$. (b) ϕ_y = 0, 2, and 4°; $d_x = d_y = \phi_x = 0$.

The theoretical variation of K vs z for the four modules constructed for delivery to the Naval Research Laboratory is shown in Figs. 7(a-d). Curves are given for d_x = 0, 1, and 2 μm. Figure 7(a) applies to Module MK2-0002; ω_{Lx} = 0.63, ω_{Ly} = 2.27, ω_F = 2.84, and λ = 0.839 μm. Figure 7(b) is for MD2-0003; ω_{Ly} = 2.38, ω_F = 2.84, and λ = 0.851 μm. Curves for Module MD2-0004 are shown in Fig. 7(c); here ω_{Lx} = 0.59, ω_{Ly} = 2.42, ω_F = 2.84, and λ = 0.845 μm. The plots for MD2-0005 are given in Fig. 7(d); the values are ω_{Lx} = 0.64,

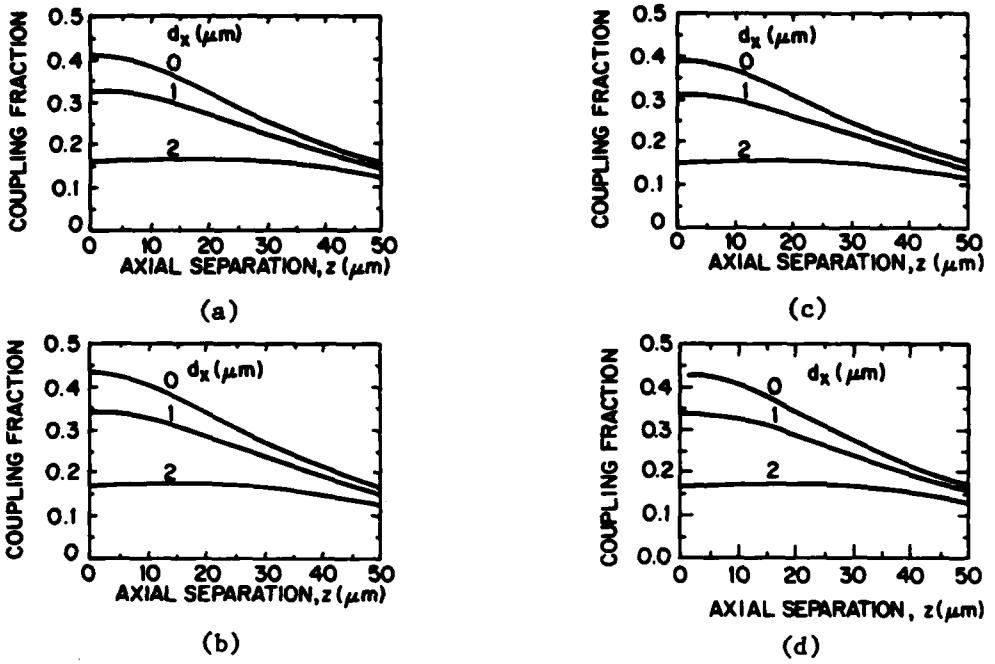

Figure 7. Calculated coupling fraction K vs axial separation z for actual modules. d_x = 0, 1, and 2 μm; $d_y = \phi_x = \phi_y = 0$. w_F = 2.84 μm.
(a) Module MK2-0002: w_{Lx} = 0.63, w_{Ly} = 2.27, λ = 0.839 (μm);
(b) Module MK2-0003: w_{Lx} = 0.66, w_{Ly} = 2.33, λ = 0.851 (μm);
(c) Module MK2-0004: w_{Lx} = 0.59, w_{Ly} = 2.42, λ = 0.845 (μm);
(d) Module MK2-0005: w_{Lx} = 0.64, w_{Ly} = 2.63, λ = 0.848 (μm).

w_{Ly} = 2.63, and λ = 0.848 μm. The coupling behavior of these modules is very close to that discussed in connection with Fig. 6(a), which shows the same family of curves for a "typical" module.

Figure 8(b) gives curves for the predicted coupling K for a cylinder lens. Plots for the radius r_x = 5, 10, 15, and 20 μm are shown. The refractive index is assumed to be 1.5. The axis of the cylinder is parallel to the lateral (y) direction, and the flat surface is in contact with the fiber end (see Fig. 1). Figure 8(a) gives similar plots for a spherical lens. Here $r_x = r_y$ and curves for $r_x = r_y$ = 5, 10, 15, and 20 μm are given.

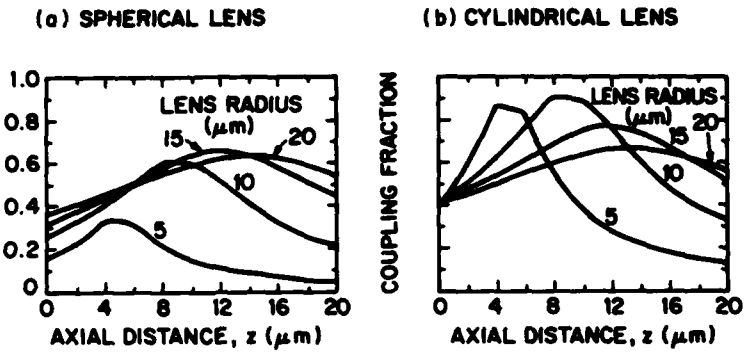

Figure 8. Calculated coupling vs z with lenses having a refractive index of n = 1.5. (a) Plano-convex spherical lens with lens radius values of 5, 10, 15, and 20 μm. (b) Plano-convex cylindrical lens with lens axis parallel to the lateral, y, direction. Lens radius values are r_x = 5, 10, 15, and 20 μm.

Whereas the cylinder lens has the potential for giving coupling fractions near 0.9, the spherical lens might raise the fraction to approximately 0.65. Obtaining the highest efficiencies with the cylindrical lens requires a radius between 5 and 10 μm and imposes a high tolerance on the axial location. We would expect that a coupling less stable than butt coupling might result. The spherical lens case is more tolerant but provides a lower coupling fraction. Cylinder lenses with radii larger than optimum might be considered as a compromise between coupling efficiency and axial position tolerance. For example, a cylindrical lens with r_x between 15 and 20 μm would provide a coupling fraction of about 0.7 and axial positioning tolerance of approximately ±5 μm.

At this point, the results of our analyses of coupling may be summarized as follows: The maximum coupling fraction available to us when we use a typical high-power CDH-LOC laser butt-coupled to a single-mode fiber will be about 0.4 (not taking Fresnel reflection into account). The axial separation sensitivity can be kept relatively low. K changes by less than 0.01 per micrometer at a distance z ≅ 10 μm (approximately 0.0005 in.). The angular sensitivity in the lateral direction (y tilt) (slope $dK/d\phi_y$ = 0.1/degree) is

high and will require control to approximately 0.5°. The coupling is also very sensitive to both transverse and lateral offsets. The slope near d_x = 1 μm is dK/dd_x = 0.15 μm. Thus, it is highly desirable to control the offsets to fractions of a micrometer. In the case of lens coupling, similar offset sensitivities are expected.

In the next section we are considering the design of a coupling module to meet these requirements.

SECTION III

DESIGN OF COUPLING MODULE

A. DESIGN ALTERNATIVES

During the course of this program we considered several design alternatives. We faced the following conditions: High-power laser chips available to us are indium bonded to copper L-mounts. The lateral positioning accuracy with respect to a fixed fiducial (such as the side of the L-mount) is of the order of ±50 μm. Transverse positional accuracy is on the order of ±5 μm. This is due to variations in both the growth layers and indium solder thickness. In addition to these large uncertainties in the laser diode position, we have to contend with uncertainty in the fiber module position. The tolerance on the core-cladding concentricity is claimed to be ±1.5 μm. The cladding diameter is held to ±2.5 μm. Also, it is necessary to protect the fiber tip by placing the fiber in a ferrule. The ferrule itself must be positioned in a holder that allows axial motion. The ferrule inner diameter is 130 μm, while the fiber-cladding outer diameter is 125 μm. The sliding fit of the ferrule inside the fiber-ferrule holder can, at best, be held to ±5 μm. We would thus anticipate an average core-position uncertainty of the order of ±5 μm.

Because of these uncertainties in the position of the laser and the fiber, it is impossible to design a fixed structure in which the positions of the laser and the fiber are predetermined.

To overcome these problems we considered two general types of approaches. The first type consisted of positioning the fiber and the laser by external mechanical means and then permanently fastening them in place at the optimum coupling position. This had been tried by Ladany et al. [3]. Following this approach, we generated a flanged modular structure. We intended to use an epoxy bond to seal the flanged unit holding the fiber to the flanged unit holding the laser. Soon, however, experiments with the flanged module showed that there was sufficient transverse motion during bonding to make the results unreliable. This, as well as some experience with the long-term mechanical instability of earlier related designs, led us to abandon this general approach.

The second type of approach we considered and implemented was to provide means for postassembly adjustment of the module. An initial design was based

on eccentric motion similar to that first described by Krumpholz [10]. However, we found that the required positioning tolerances were not readily achieved this way. In addition, the actual adjustment motion required a special external jig and was awkward.

The approach we finally chose provides a solution to the postassembly-positioning problem: We used tapered rods driven by screws to move spring-loaded beams. This method allows motions to be made after the elements are assembled in a package or module. The module thus obtained is small and stable, has high resolution, and can be manufactured by conventional machine-shop techniques.

Figure 9 shows a schematic diagram of our design of a device to provide microtranslation in the x direction (microtranslator). The upper plate is moved with respect to the base when the taper section of the taper screw is driven in the y direction by turning the taper screw. To make the motion smooth and repeatable, the taper section passes through the opening formed by a V groove in the upper plate and another V groove in the base. The distance, L_2, in which the taper screw is free to flex is made sufficiently long so that the screw will not bind or take a permanent set as it "rides up" the base V groove. The upper plate is securely attached to the base by screws. As the taper advances to the right, the laser or fiber holder describes an arc, as the heavy right portion of the upper plate of thickness T_1 substantially does not bend while the spring section of thickness T_2 and length L_S flexes. The shape of the spring section may be chosen to meet the particular stress and stability requirements of different applications. In this version, T_2 is chosen equal to the thickness of the fastening region T_3. This simplifies the machining. If the distance L_1 is large compared with the displacement caused by the taper, the motion at the laser or the fiber holder may be considered substantially a translation in the x direction. Further, the motion at the laser or the fiber holder will be reduced from that at the V groove by L_1/L_2. We refer to this device as the MK2 microtranslator. (In our first version, MK1, we had used a round hole rather than a V groove to receive the taper screw. But the taper screw tended to bind in the round hole, causing very erratic operation.)

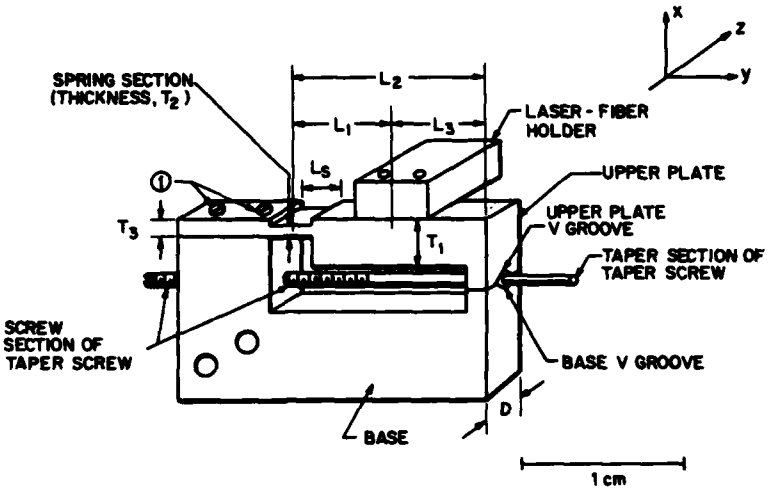

Figure 9. Schematic drawing of spring-loaded taper-screw microtranslator.

B. CALCULATION OF MECHANICAL AND THERMAL REQUIREMENTS

To ensure stable operation of the microtranslator in a coupling module that is to be moved around, it is important that the force required to move the arm be high compared with any inertial or gravitational forces that may be developed on the arm and the laser or fiber mount. We consider the spring section to be a simple beam. For this case, the moment of force around the center of the spring section required for a deflection angle α is given by [11]

$$M = \alpha\, D(L_S)^3\, E/(12\, L_2) \tag{1}$$

E is Young's modulus and D is width (see Fig. 9). The force, F, is given by

$$F = M/L_2 \tag{2}$$

It is convenient intuitively to give the force in kg-weight units. For Young's modulus in dynes/cm^2, the force in units of kilogram-weight (kg-wt) is

$$F = \alpha\, D(L_S)^3\, E/(12\, L_2 \times 9.8 \times 10^5) \tag{3}$$

Here all the lengths are in centimeters.

It is also important to know the maximum stress to avoid exceeding the yield point and/or maximum stress limit of the spring section. The maximum stress occurs at the so called outer fiber. In our case this is the lower surface (in the y-z plane) of the spring when the taper is driven its maximum distance into the V grooves. This maximum stress, σ_x, is given by

$$\sigma_x = \alpha L_S E/2 \tag{4}$$

We use the geometric relations and consider changes in the x position at the laser or fiber location. For a change in x of Δx,

$$\alpha = \Delta x/L_1 \tag{5}$$

We are now able to calculate both the force and maximum stress using Eqs. 3, 4, and 5.

In addition to being concerned about the forces and stresses, we must also consider the effect of temperature variations. The laser diodes are mounted on copper mounts to provide high thermal conductivity. The thermal expansion coefficient of copper is approximately 16 x 10^{-6}/°C at room temperature. To be compatible with this, we chose phosphor bronze as the material to make the spring and body of the microtranslator. The thermal expansion coefficient of phosphor bronze (97.8 Cu, 2 Sn, 0.2 P) is 16.8 x 10^{-6}/°C [12]. We chose #416 stainless steel for the taper screw because of its hardness and ability to be polished. Its thermal expansion coefficient is about 16 x 10^{-6}/°C. We selected these materials for the good match in their thermal properties so that temperature-induced relative motion among the parts would be minimized.

Copper bronzes (such as phosphor bronze) in spring-plate form have a Young's modulus of approximately 11 x 10^{11} dynes/cm^2 and tensile strengths in the 20-70 x 10^8 dynes/cm^2 range [13]. We chose a standard #1-72 (72 turns/in.) machine screw. The taper portion is ground with a taper of 1°. The dimensions chosen are as follows: L_1 = 0.72 cm, L_2 = 1.4 cm, L_3 = 0.68 cm, D = 0.5 cm, L_S = 0.25 cm, and $T_3 = T_2$ = 0.125 cm.

In Fig. 10 the required force in kg-wt and the maximum stress in units of 10^8 dynes/cm^2 are shown as a function of the deflection in micrometers (μm). The number of turns of the taper screw corresponding to the deflection is also shown on the top of the figure. The calculated slope is 145 g/μm. As can be

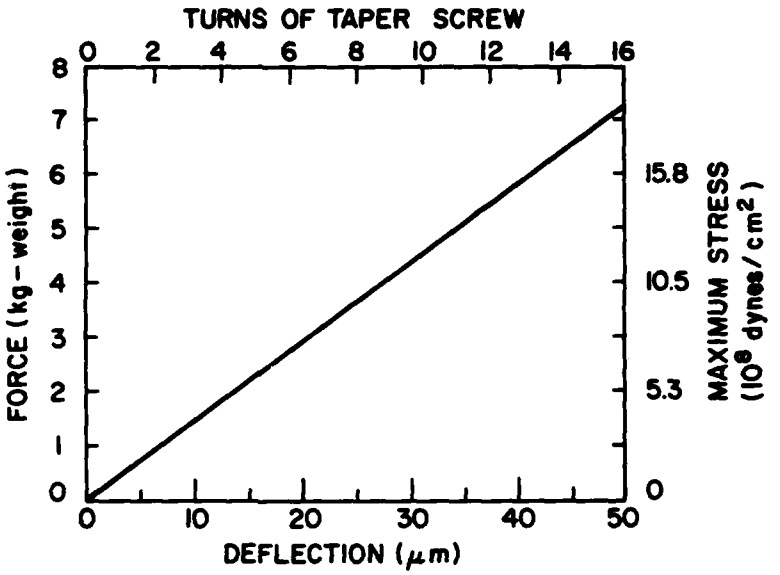

Figure 10. Calculated force required to deflect microtranslator of Fig. 9 vs deflection. Right-hand scale gives maximum stress. Upper scale gives number of turns of taper screw corresponding to deflection. The slope is 0.145 (kg-wt)/μm. The deflection plotted is at the laser-fiber holder position.

seen, the maximum stress approaches 20 x 10^8 dynes/cm^2 at 50-μm deflection. The 145 g-wt required for 1.0-μm deflection is adequate. This may be seen by considering that mass supported on the arm, including the arm mass, is approximately 10 g. Assume that the module is subjected to an acceleration of from 0 to 100 km/h in one second. This corresponds to four times the acceleration due to gravity. The acceleration applied to 10 g gives a force of 40 g-wt, which would cause a deflection of only 0.28 μm (2800 Å). In the above example, we assume that the acceleration is directed along the compliant direction of the microtranslator (x axis of Fig. 9).

We considered the resolution to be that motion which corresponds to 1/20th of a turn of the taper screw. We calculated Δx as 3.1 μm/turn. Using a measuring microscope, on one sample we found Δx to be 3.5 ± 1.4 μm/turn; on a second sample, Δx was 3.7 ± 1.4 μm/turn. The standard deviation is believed to be due to both the measurement method, which depends on accurate focus, and to some irregularities in the taper. Nonetheless, the motion in 1/20th of a turn is of the order of 0.2 μm (2000 Å).

As discussed in Section IV, the microtranslators have shown the required stability and resolution, judged by the coupling results.

C. DESCRIPTION OF COMPLETE MICROCOUPLER MODULE

The complete microcoupler module is shown in Fig. 11. Here, two microtranslators of the type shown in Fig. 9 are combined to provide relative motion between the fiber and the laser diode in both the transverse (x) and lateral (y) directions.

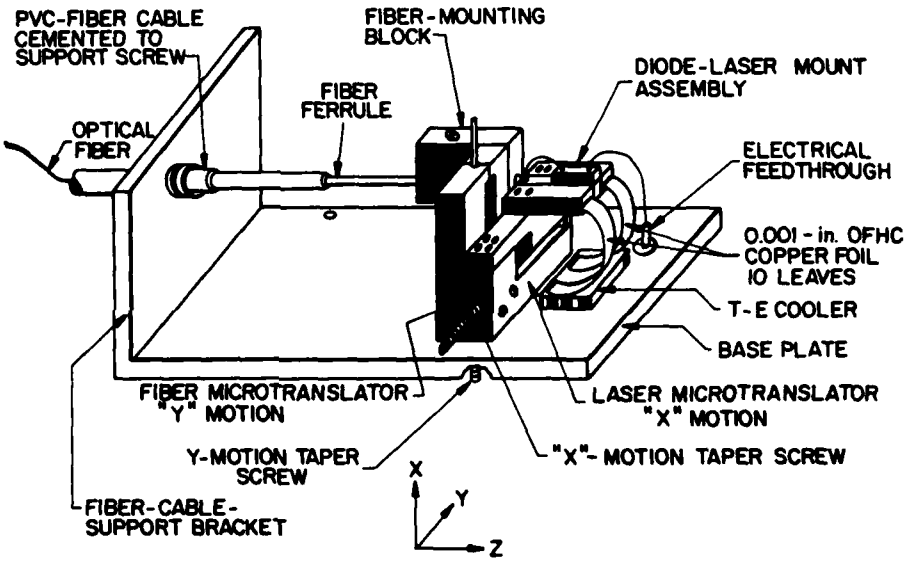

Figure 11. View of coupling module. A clamp and an electrical connection for the thermoelectric (TE) cooler are omitted for clarity.

The simple buffered single-mode fiber is made up into a cabled pigtail. The input fiber end is bonded inside a stainless-steel ferrule by means of a clear epoxy. After bonding, the fiber end is polished flush with the ferrule end. The output end of the fiber cable (pigtail) also terminates in a ferrule. Here, however, 10 cm of the fiber cladding is exposed and coated with a cladding-mode stripper before the cable is completed. The fiber buffer layer is removed for this purpose. The fibers tend to weaken when the buffer layer is removed. Thus, the output end section is protected by a relatively rigid length of clear plastic over the length of cladding-mode-stripped fiber. The

length of fiber between the input ferrule and the mode-stripper section is protected by a PVC jacket that is cemented to the ferrule at the input end, and the stiff plastic sleeve at the output end. The fiber input ferrule is securely held on the fiber mounting block by set screws, tightened after adjustment of the axial position.

The fiber mounting block is fastened to the fiber microtranslator, which is positioned so that motion of its taper screw provides y motion of the fiber. The CDH-LOC laser is bonded to an L-mount that is held in the diode-laser-mount assembly. The L-mount is clamped by a set screw between two copper pieces that are fastened to the laser microtranslator. This assembly is positioned so that motion of its taper screw moves the laser in the x direction. The fiber microtranslator is fastened to the laser microtranslator with machine screws and this combination, in turn, is fastened to a base plate that allows access to the y-motion taper screw by means of an opening. The z distance between the fiber end and the laser is adjusted during assembly by moving the fiber ferrule in the fiber mounting block to obtain the correct spacing. A long hollow screw through which the fiber cable passes is placed in the end plate for this adjustment. This screw is replaced with a short screw to which the cable is cemented when the adjustment is completed.

The laser-diode mount is temperature stabilized by being thermally coupled to a thermoelectric cooler through 10 OFHC copper strips each 0.5 cm (0.2 in.) wide, 0.0025 cm (0.001 in.) thick, and 1 cm (0.4 in.) long. The foils are soldered to the two copper pieces that clamp the laser L-mount. At the thermoelectric cooler end, the foils are soldered to a copper bar that is pressed by a clamp to the "cool" plate of the cooler. The clamp also keeps the "hot" plate of the cooler in good contact with the massive base plate. The clamps and electrical connections for the cooler are not shown in Fig. 11.

We calculate that there will be a temperature rise of 1.2°C from the cooler to the laser mount at a laser current of 300 mA. This current is well above the average operating current of the lasers used in our program. The entire microcoupler module is self-contained and is provided with a sealing cover that allows access to the taper screws. The cover may be adapted to completely encapsulate the microcoupler. If that is done, provision could be made for the screws to be rotated by "O"-ring-sealed shafts. An attractive possibility of this arrangement is the use of miniature servo-motors to turn

the screws. In this case feedback circuits might be employed to control the positioning.

We point out that our approach of having the laser moved in one direction by one microtranslator and the fiber moved in an orthogonal direction by a second microtranslator overcomes the difficulty of having a micropositioner move one of the devices (laser or fiber) in two orthogonal directions. This allows us to use the simple microtranslator illustrated in Fig. 9.

SECTION IV

RESULTS AND DISCUSSION

A. MODULE-COUPLING MEASUREMENTS

Tracings of x-y recorder plots of the cw fiber output vs laser current (solid line) and the coupling fraction (round points connected by line segments) for four complete modules are given in Figs. 12, 13, 14, and 15. The coupling fractions are calculated from current-power plots made on the direct-front-facet laser output. The plot shown in Fig. 16 of the direct-front-facet output power for the laser used in Module MK2-0003 is typical.

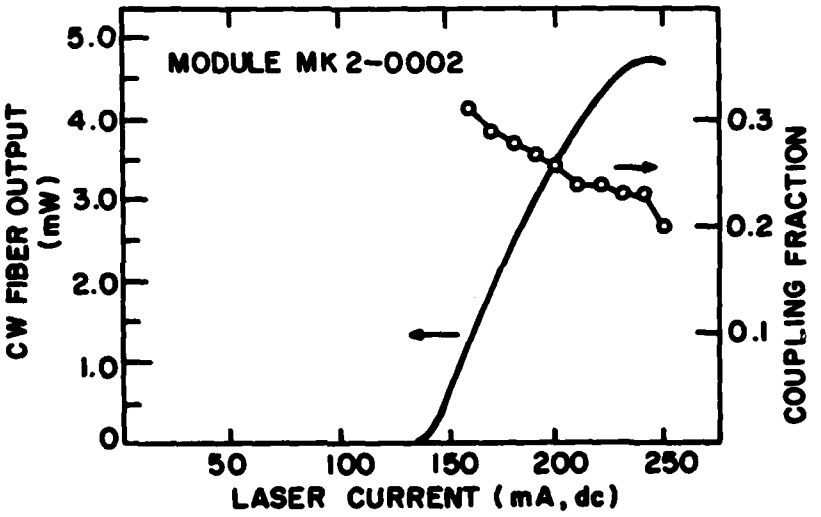

Figure 12. CW fiber output vs laser current (solid line and left scale). Coupling fraction (round points and right scale). Coupling module MK2-0002.

As can be seen from the figures, the maximum cw power obtained with MK2-0002 is 4.6 mW. The maximum for MK2-0003 is 4.7 mW. MK2-0004 reached a maximum of 7.3 mW and MK2-0005 reached 7.7 mW, the highest cw power coupled into a single-mode fiber we have yet obtained. This is also, to the best of our knowledge, the highest cw power ever coupled by an means from a laser to a single-mode fiber.

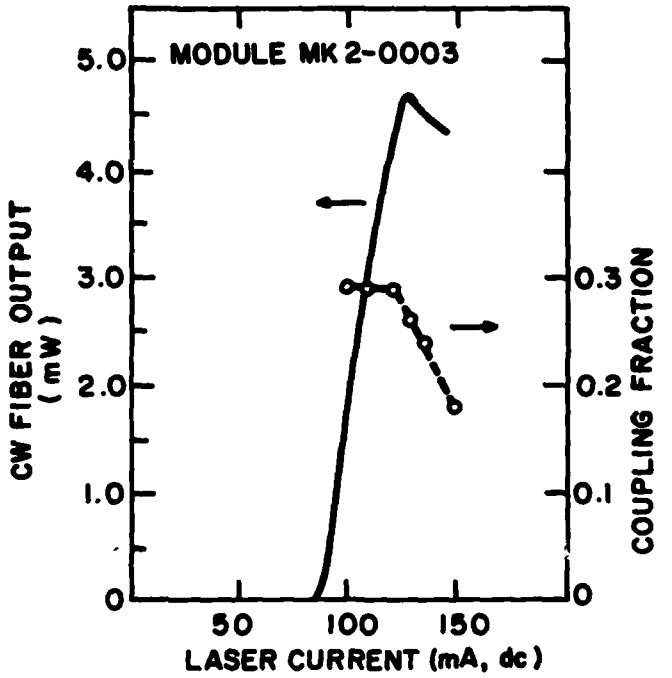

Figure 13. CW fiber output vs laser current (solid line and left scale). Coupling fraction (round points and right scale). Coupling module MK2-0003.

The coupling fractions for all four of these modules vary slowly with current in roughly the 0.2-0.4 range. All modules show a decided drop in coupling fraction as the laser current is increased beyond a certain point. This observation is discussed at greater length below. The coupling fractions as plotted in Figs. 12-15 are not corrected for Fresnel reflections from the fiber ends.

The peak fiber output power of Module MK2-0004 operated at a 100-ns 50%-duty-cycle pulse with 80 mA of dc bias is given in Fig. 17. Here the maximum peak value at the fiber output end is 9.1 mW.

A summary of the module characteristics is given in Table 1. The CDH-LOC lasers used on these modules have been described in detail in Refs. 7-9.

The laser beam waists were obtained from far-field measurements. Typical of these is the far field of the laser used in Module MK2-0003, which is shown in Fig. 18. The values given in Table 1 are those measured at a laser output of 20 mW cw and are averaged over far-field angles measured at the half-power, 1/e power, and $1/e^2$ power points [9].

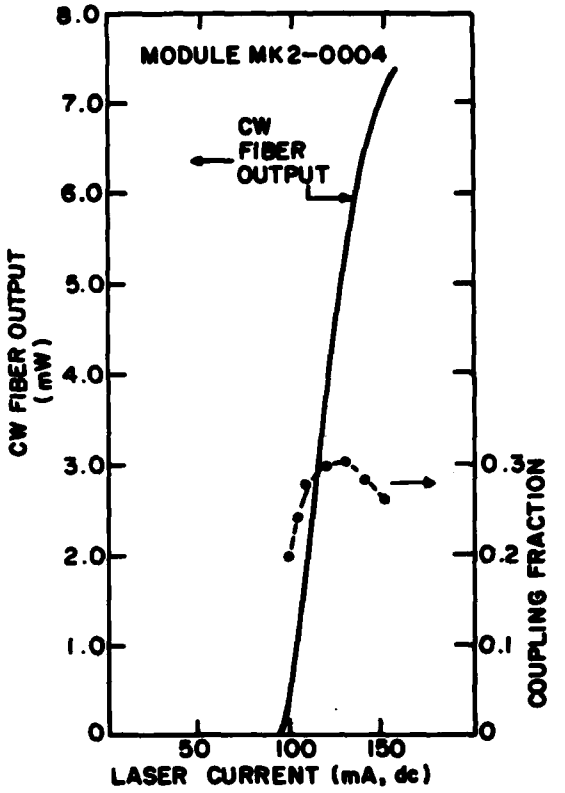

Figure 14. CW fiber output vs laser current (solid line and left scale). Coupling fraction (round points and right scale). Module MK2-0004.

The high values of cw power observed in the four modules is consistent with the high-power capabilities of the CDH-LOC lasers and the choice of beam waist sizes for both the fiber and the lasers. The peak values of measured coupling fraction shown in Table 1 are corrected for Fresnel reflection from both fiber ends at 4% reflection per end.

These values are in reasonable agreement with the values calculated from theory. Comparison with Figs. 4-7 indicates that any discrepancies could be due to tilts of the order of 1°. The adjustable feature of the modules allows us to maximize the coupling with respect to offset, but not to adjust for tilt after the module has been assembled.

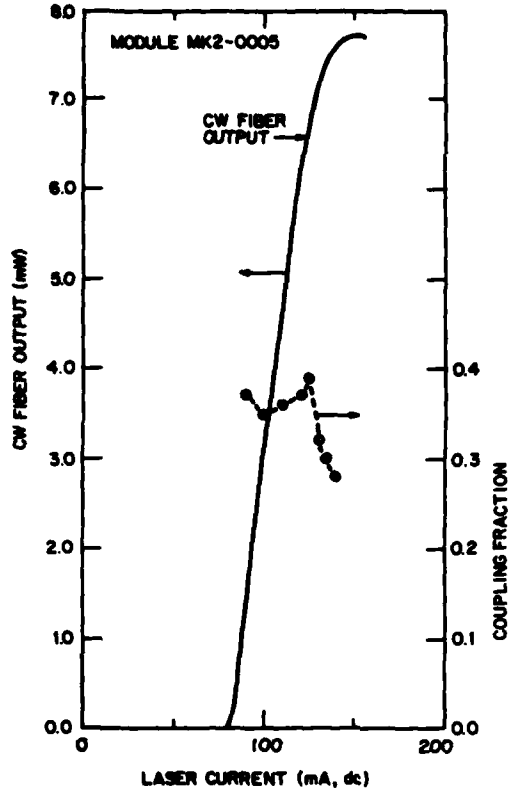

Figure 15. CW fiber output vs laser current (solid line and left scale). Coupling fraction (round points and right scale). Module MK2-0005.

The reduction of coupling efficiency as the current is raised beyond a certain point severely restricts the coupling to the fiber at high laser outputs. We note that this coupling roll-off occurs at approximately 200 mA in MK2-0002, in which we use a laser with a rather high threshold current. The roll-off occurs at approximately 125 mA in MK2-0003, MK2-0004, and MK2-0005. The laser output power at which the roll-off occurs is in the 15- to 20-mW range.

We believe this effect to be due to a reflection-enhanced multimoding instability at high output powers. The power fraction coupled back into the laser mode due to Fresnel reflection from the input fiber end has been calculated and is shown in Fig. 19. As can be seen for the axial separations of about 10 μm used in our modules, about 0.006 (0.6%) of the power is reflected into the laser mode.

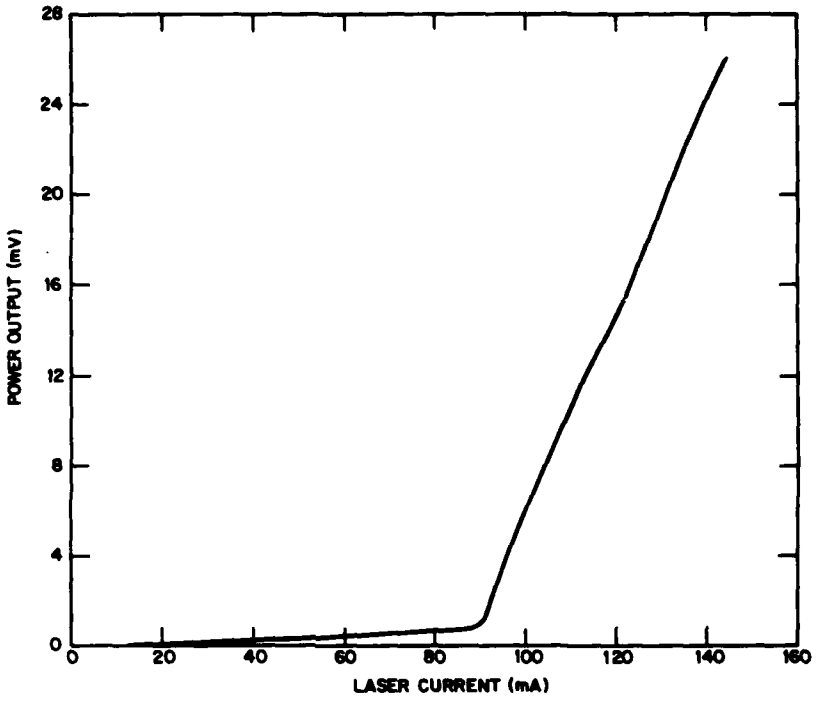

Figure 16. Direct cw laser output vs current for the CDH-LOC laser used in Module MK2-0003. The soft "kink" in the 120- to 130-mA region is associated with the roll-off of coupling fraction in the modules.

At laser outputs of about 20 mW, approximately 100 μW of power is thus reintroduced into the laser mode. It is well known that a variety of instabilities have been observed in diode lasers subjected to such reflection [14-17]. Important changes in output coupling due to external Fabry-Pérot effects are described in Refs. 9 and 18.

The tendency in these lasers toward multimoding at high power levels is implied by the far-field plots of Fig. 18. The change in lateral far field between 10 and 20 mW is apparent. At 10 mW, the half-power far-field width is approximately 8°; at 20 mW, it increases to approximately 10°. The changes imply a decrease in beam waist from about 2.5 to 2.1 μm. For a simple change of this order, the size of the lateral mode is insufficient to explain the observed in drop in coupling fraction. Additional evidence on the moding situation is given by the spectral output. The spectral output of the laser

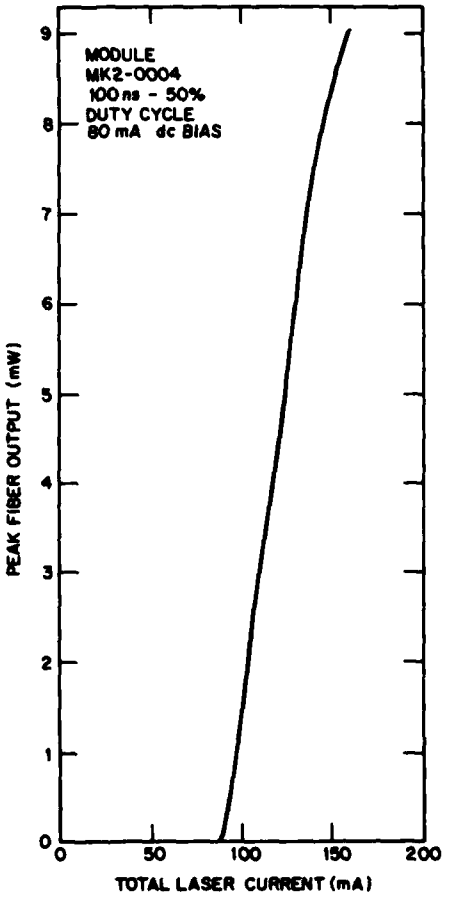

Figure 17. Peak fiber output vs total laser current. The laser is operated with 80-mA, dc bias and 100-ns 50%-duty-cycle pulses. Module MK2-0004.

used in Module MK2-0003 before coupling is shown in Fig. 20. The output consists of a single longitudinal (wavelength) mode centered at 8508 Å. The spectrum is shown at a laser current of 130 mA, dc (20-mW cw output). The isolated laser, however, operates in a single longitudinal mode over the entire range of current we are considering. The spectrum of the light coming out of the fiber is shown for a laser current of I = 110 mA (~10 mW cw) in Fig. 21 and I = 130 mA cw) 130 (~20 mW cw) in Fig. 22. Note that compared with Fig. 20, in Figs. 21 and 22 the laser is apparently oscillating in more than a single longitudinal mode. At I = 110 mA, the graph shows four relatively strong lines between 8479 and 8468 Å. These lines are equally spaced at the laser-cavity/Fabry-Pérot spacing of 3.7 Å. At I = 130 mA, in addition to the four

TABLE 1. SUMMARY OF MODULE CHARACTERISTICS

Module	CDH-LOC Laser Beam Waists ω_{Lx} (μm)	CDH-LOC Laser Beam Waists ω_{Ly} (μm)	Wavelength, λ (μm)	Measured Axial Spacing, z (μm)	Maximum Fiber Output, cw (mW)	Coupling Fraction Calculated from Fig. 7	Measured Max. Coupling Corrected for Fresnel Reflections
MK2-0002	0.63	2.27	0.839	14	4.6	0.37	0.34
MK2-0003	0.66	2.33	0.851	10	4.7	0.41	0.31
MK2-0004	0.59	2.42	0.845	9	7.3	0.38	0.33
MK2-0005	0.64	2.63	0.848	10	7.7	0.40	0.41

Note: The fiber used in all the modules was a Corning 43650-V01 (Corning Glass Works, Corning, NY). Nominal core diameter was 4.5 μm; measured fiber beam waist was ω_F = 2.84 μm; effective step-index change, Δn/n, was 0.0025.

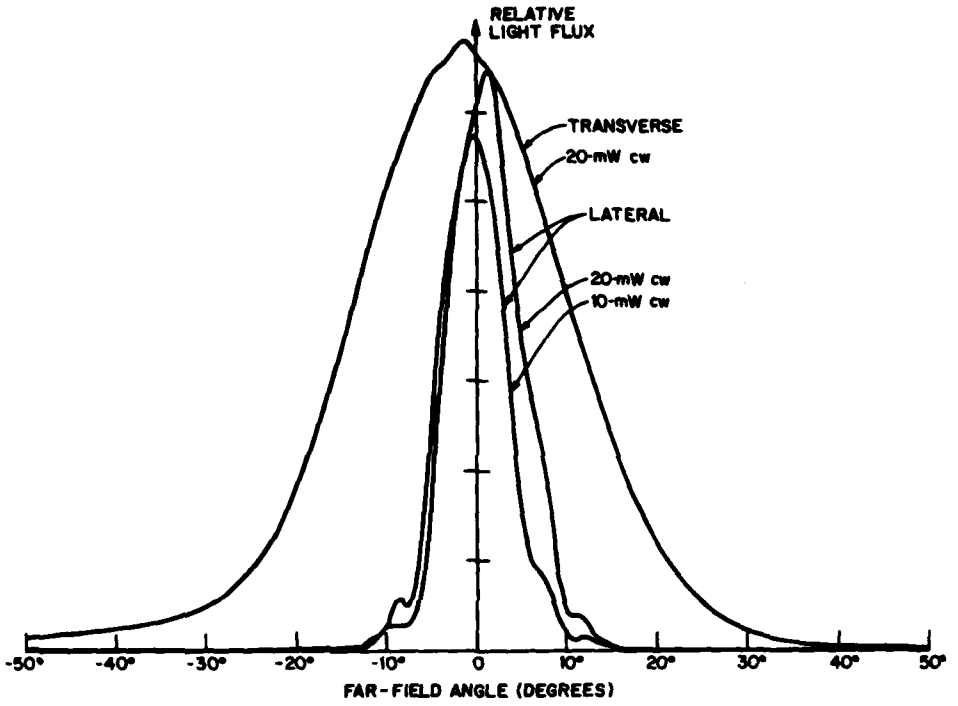

Figure 18. *Far fields of the CDH-LOC laser used in Module MK2-0003. Note the difference in lateral far fields for I = 110 mA (10 mW) compared with I = 130 mA (20 mW).*

strong, equally spaced, Fabry-Pérot lines that are now shifted to lie between 8477 and 8466 Å, there is a weak pair of lines (8454 and 8458 Å) that are spaced further apart from each other (4 Å compared with 3.7 Å) and whose spacing of 8 Å from the principal set is not an integral multiple of 3.7 Å. This is clear evidence that an additional spatial mode, oscillating in its own set of longitudinal modes, is present at I = 130 mA -- a mode that is absent at 110 mA.

In addition, note that the direct laser output power vs current curve (Fig. 17) shows a soft "kink" at around I = 125 mA. Such kinks have been identified as being associated with the onset of additional spatial modes. Similar observations have been made on all of the modules discussed above.

We, therefore, conclude that the roll-off of coupling efficiency above I ∿ 125 mA for Modules MK2-0003, -0004, and -0005, and above I ∿ 190 mA for MK2-0002, is due to the emergence of a second spatial mode at high operating levels. We also believe that this behavior is encouraged, if not caused, by

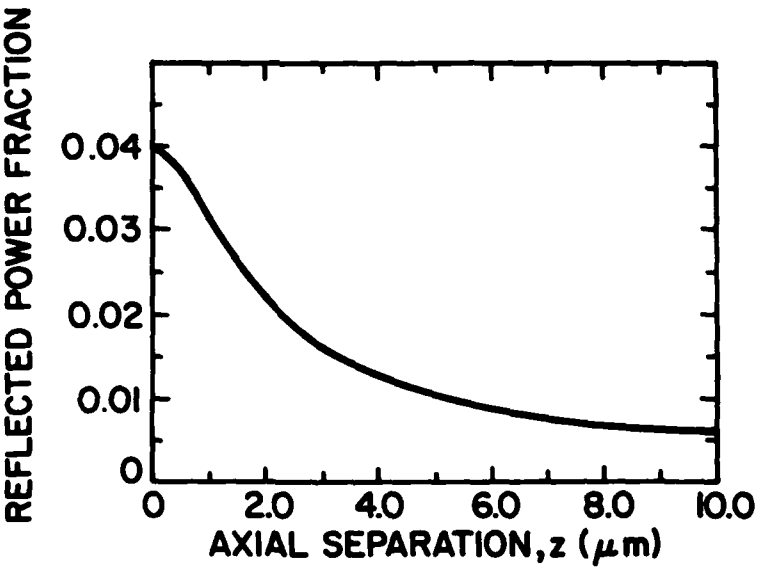

Figure 19. Calculated reflected power fraction vs axial separation z. A 4% Fresnel reflection from the fiber end facing the laser is assumed. The power fraction here is the fraction of the reflected light coupled into the laser mode for a typical CDH-LOC laser (see Fig. 4 caption).

the direct reflection from the input end of the fiber into the laser. This reflection can be reduced if either spherical or cylindrical lens coupling rather than simple butt coupling is used.

The modules described in this report are the ones that are being delivered to NRL under this contract. The module covers allow access to the taper screws. These may be turned with a small screwdriver or video tuning tool. The output remains constant after adjustment. We have subjected the modules to mild mechanical shock, such as tapping the far plate with a screwdriver and bending the cable, and could see no change in output either during or after these actions.

B. LENS COUPLING

We have made some initial attempts at coupling using cylinder lenses drawn from glass rods to diameters in the 10- to 20-μm range. These were positioned over the end of the single-mode fiber under a microscope. The fiber was illuminated with incoherent light from the output end so that the cylinder lens could be centered on the core. The lens was cemented in place with optical

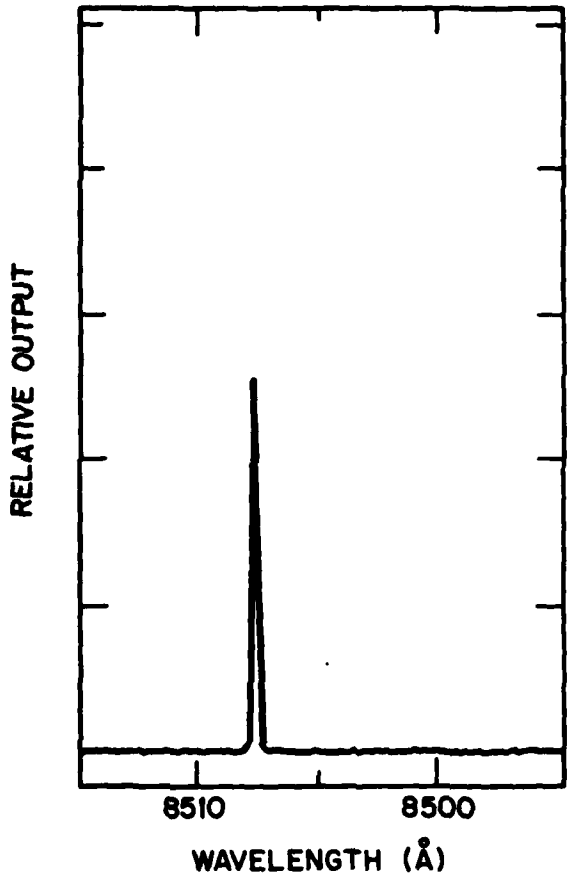

Figure 20. Spectrum of direct output from CDH-LOC laser used in Module MK2-0003. The current is 130 mA, dc. A single-wavelength mode remains over the range of currents studied.

epoxy. However, judging by far-field measurements made on the lensed fiber, we found it difficult to center the lens with sufficient accuracy. Also, we were unable during this work to cement the lens onto the fiber with a bond strong enough to withstand normal handling. We do believe that further investigation of lens coupling is worthwhile.

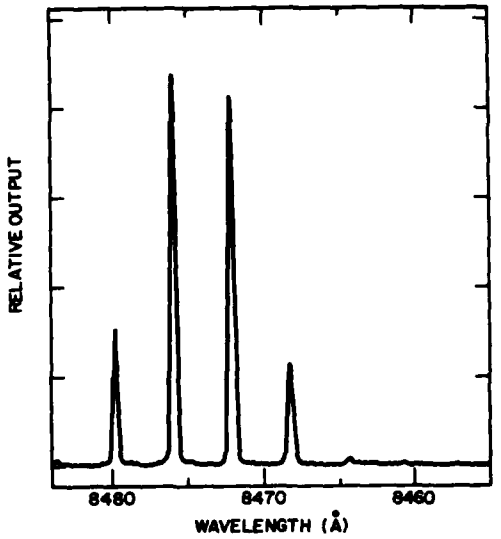

Figure 21. Spectrum of fiber output at laser current of 110 mA, dc. Module MK2-0003. A single group of lines spaced at the laser-cavity/Fabry-Pérot separation is apparent.

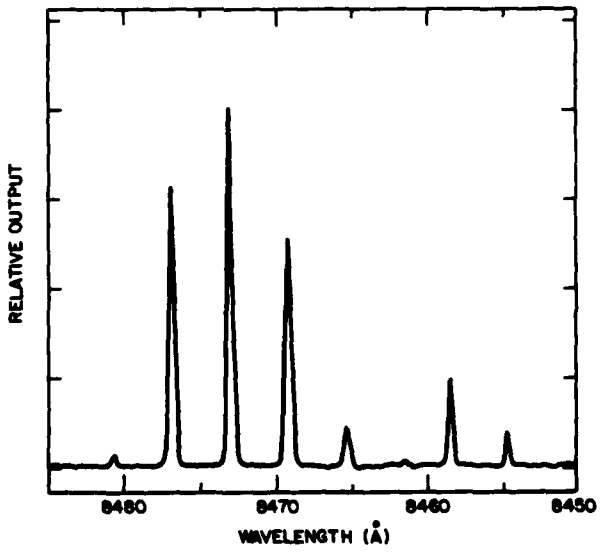

Figure 22. Spectrum of fiber output at laser current of 130 mA, dc. Module MK2-0003. Compared with Fig. 21, a second group of lines appears.

SECTION V

CONCLUSIONS

We have developed a unique and adjustable module capable of coupling high power from a semiconductor laser to a single-mode fiber. CW powers of over 7.5 mW have been coupled into the fibers with 30% or greater coupling efficiencies. The observed cw coupled powers are much greater than previously reported results. The modules allow adjustment of both the lateral and transverse fiber-laser offsets. This is done by use of a novel micropositioner incorporated into the module. Thus, long-term drifts in coupling that may occur -- for example, during laser aging or due to temperature extremes -- can be readily compensated for by turning two controls. The adjustments may be adapted for use with miniature servo-motors so that the coupling may be controlled automatically.

The modules are rugged, being resistant to moderate shock and fiber motion; they are also stable and compact. Provision is made for laser temperature stabilization with a thermoelectric cooler. The internal microtranslators provide x-y motion by moving the laser in the transverse (x) direction and the fiber in the lateral (y) direction. The translators have a resolution of 2000 Å. These novel miniature spring-loaded taper-screw microtranslators have potential use in a variety of positioning applications. In particular, they can meet the positioning requirements in laser-planar and stripe-waveguide couplers, as well as in waveguide-waveguide, fiber-waveguide, and fiber-fiber couplers.

REFERENCES

1. H. Kogelnik, Proceedings of the Symposium on Quasi-Optics, New York Polytechnic Institute, New York, 1964, pp. 333-347.
2. L. G. Cohen, Bell Syst. Tech. J., 51, 573 (1972).
3. I. Ladany, H. J. Wolkstein, R. S. Crandall, and D. R. Patterson, "Ultra High Speed Modulation Studies of Injection Lasers," Final Report under Contract No. N00173-77-C-0136, Naval Research Laboratory, June 1978.
4. J.-I. Sakai and T. Kimura, IEEE J. Quantum Electron., QE-16, 1059 (1980).
5. M. Saruwatari and T. Sugie, IEEE J. Quantum Electron., QE-17, 1021 (1981).
6. R. E. Wagner and W. J. Tomlinson, Appl. Opt., 21, 2671 (1982).
7. D. Botez, Appl. Phys. Lett., 36, 190 (1980).
8. D. Botez and J. C. Connolly, Appl. Phys. Lett., 38, 658 (1981).
9. J. M. Hammer, C. C. Neil, D. Botez, and J. C. Connolly, "Coupling of Junction Lasers to Thin-Film Optical Waveguides," Final Report under Contract No. N00173-80-C-0440, Naval Research Laboratory, Nov. 1981, pp. 24-25.
10. O. Krumpholz, Paper WB-5, Digest, Topical Meeting on Integrated Optics - Guided Waves, Materials and Devices, Las Vegas, Nev. (Feb. 1982).
11. S. Timoshinko, Strength of Materials, 2nd ed., D. Van Nostrand, New York, 1940, Chapt. IV, pp. 83 et seq.
12. C. D. Hodgman, Ed., Handbook of Chemistry and Physics, 38th ed., Chemical Rubber Publishing Co., Cleveland, O., 1956, p. 2060.
13. D. E. Gray, Ed., American Institute of Physics Handbook, 2nd ed., McGraw-Hill, New York, 1963, pp. 2-64.
14. O. Hirota and Y. Suematsu, IEEE J. Quantum Electron., QE-15, 142 (1979).
15. K. Kobayashi and M. Seki, IEEE J. Quantum Electron., QE-16, 11 (1980).
16. R. Lang and K. Kobayashi, IEEE J. Quantum Electron., QE-16, 347 (1980).
17. L. Goldberg, H. F. Taylor, A. Dandridge, J. F. Weller, and R. O. Miles, IEEE J. Quantum Electron., QE-18, 555 (1982).
18. J. M. Hammer and C. C. Neil, IEEE J. Quantum Electron., QE-18, 1751 (1982).


DA
FIL